Synthesis, Characterization, Langmuir−Blodgett Film-Forming Properties, and Second-Harmonic-Generation Studies of Ruthenium(II) Complexes with Long Hydrocarbon Chains

Ben Wai-Kin Chu and Vivian Wing-Wah Yam*

Department of Chemistry, The University of Hong Kong, Pokfulam Road, Hong Kong, People's Republic of China

Received November 27, 2000

Several ruthenium(II) surfactants of general formula $[Ru(bpy)_2L]^{2+}$ [L = *N*-(2-pyridylmethylene)-3,4-bis(tetradecyloxy)benzenamine, *N*-(2-pyridylmethylene)-3,4-bis(octadecyloxy)benzenamine, 9-(3,4-bis(tetradecyloxy)-benzenamino)-4,5-diazafluorene, 9-(4-(tetradecyloxy)-4′-azabenzenamino)-4,5-diazafluorene, 4,7-dinonadecyl-1,10-phenanthroline] and $[Ru(L)_3]^{2+}$ (L = 4,7-dinonadecyl-1,10-phenanthroline) were synthesized and characterized by elemental analysis, ^{1}H NMR, UV−vis, luminescence spectroscopy, and cyclic voltammetry. Their Langmuir−Blodgett (LB) film formation properties and surface pressure−area (π−*A*) isotherms were also studied. Two complexes were found to show second-harmonic-generation (SHG) behavior.

Introduction

The Langmuir−Blodgett (LB) technique has been used to construct organized systems for efficient energy and electron transfer.[1] Its application in making nonlinear optical (NLO) materials[2] may attract some interest because of the potential in making ordered ultrathin films in which molecular orientations and packings can be highly controlled.[3] Transition metal complexes offer several advantages over organic compounds by possessing metal-to-ligand charge transfer (MLCT) transition or ligand-to-metal charge transfer (LMCT) transition in the visible region, which have been shown to be important for the second-harmonic-generation (SHG) process.[4] They also offer low-energy excited states with excited-state dipole moments significantly different from their respective ground-state dipole moments, redox-active metal centers, high environmental stability, high solubilities in common solvents, and wide choice of ligands for fine-tuning and optimizing the first molecular hyperpolarizability of a particular system.[5]

Ruthenium(II) bipyridyl complexes are excellent photosensitizers for artificial photosynthetic systems as well as for optoelectronic applications due to their rich photochemical behavior and diversity of coordination forms.[6] In this paper, we describe the synthesis of several new amphiphilic ruthenium(II) bipyridyl complexes with ligands bearing long hydrocarbon tails. Their photophysical, electrochemical, and LB film-forming properties and pressure−area (π−*A*) isotherms have been studied. Two of the complexes have also been found to show SHG activities.

Experimental Section

Materials and Reagents. Analytical reagent grade solvents and compounds were used for preparations. 2-Pyridinecarboxyaldehyde was freshly distilled under reduced pressure before use. *cis*-$[Ru(bpy)_2Cl_2]$,[7] 4,5-diazafluoren-9-one,[8] 3,4-bis(tetradecyloxy)aniline,[9] 3,4-bis(octadecyloxy)aniline,[8] 9-(3,4-bis(tetradecyloxy)benzenamino)-4,5-diazafluorene[8,9] (**L3**, Scheme 1), 9-(4-(tetradecyloxy)-4′-azabenzenamino)-4,5-diazafluorene[8−11] (**L4**), and 4,7-dinonadecyl-1,10-phenanthroline[12] (**L5**) were prepared according to literature methods. Acetonitrile for physical measurements was distilled over calcium hydride. Tetrabutylammonium hexafluorophosphate (^{n}Bu$_4$NPF$_6$) (Aldrich, 98%) was purified by recrystallization from ethanol three times before use.

* Corresponding author. Tel: (852)2859-2153. Fax: (852)2857-1586. E-mail: wwyam@hku.hk.

(1) Blodgett, K.; Langmuir, I. *J. Phys. Rev.* **1937**, *51*, 964.
(2) (a) Chemla, D. S.; Zyss, J. *Nonlinear Optical Properties of Organic Molecules and Crystals*; Academic: Orlando, FL, **1987**; *Vols. 1, 2*. (b) *Materials for Nonlinear Optics: Chemical Perspectives*; Marder, S. R., Sohn, J. E., Stucky, G. D., Eds.; *ACS Symp. Ser.* **1991**, *455*. (c) Marder, S. R.; Kippelen, B.; Jen, A. K. Y.; Peyghambarian, N. *Nature* **1997**, *388*, 845. (d) Verbiest, T.; Houbrechts, S.; Kauranen, M.; Clays, K.; Persoons, A. *J. Mater. Chem.* **1997**, *7*, 2175.
(3) Ulman, A. *An Introduction to Ultrathin Organic Films*; Academic: New York, 1991.
(4) (a) Sakaguchi, H.; Nakamura, H.; Nagamura. T.; Ogawa, T.; Matsuo, T. *Chem. Lett.* **1989**, 1715. (b) Nagamura, T.; Sakaguchi, H.; Matsuo, T. *Thin Solid Films* **1992**, *210/211*, 162. (c) Nakano, T.; Yamada, Y.; Matsuo, T.; Yamada, S. *J. Phys. Chem. B* **1998**, *102*, 8569. (d) Yam, V. W. W.; Yang, Y.; Yang, H. P.; Cheung, K. K. *Organometallics* **1999**, *18*, 5252.
(5) (a) Long, N. J. *Angew. Chem., Int. Ed. Engl.* **1995**, *34*, 21. (b) Laidlaw, W. M.; Denning, R. G.; Verbiest, T.; Chauchard, E.; Persoons, A. *Nature (London)* **1993**, *363*, 58. (c) Laidlaw, W. M.; Denning, R. G.; Verbiest, T.; Chauchard, E.; Persoons, A. *Proc. SPIE. Int. Soc. Opt. Eng.* **1994**, *2143*, 14. (d) Dhenaut, C.; Ledoux, I.; Samuel, I. D. W.; Zyss, J.; Bourgault, M.; Le Bozec, H. *Nature (London)* **1995**, *374*, 339. (e) Whittall, I. R.; Humphrey, M. G.; Persoons, A.; Houbrechts, S. *Organometallics* **1996**, *15*, 1935. (f) Houbrechts, S.; Clays, K.; Persoons, A.; Cadierno, V.; Gamasa, M. P.; Gimeno, J. *Organometallics* **1996**, *15*, 5266. (g) Coe, B. J.; Houbrechts, S.; Asselberghs, I.; Persoons, A. *Angew. Chem., Int. Ed. Engl.* **1999**, *38*, 366.
(6) Schroder, M., Stephenson, T. A. *Comprehensive Coordination Chemistry*; Wilkinson, G., Gillard, R. D., McCleverty, J. A., Eds.; Pergamon: Oxford, 1987, *Vol. 4*.
(7) Sullivan, B. P.; Salmon, D. J.; Meyer, T. J. *Inorg. Chem.* **1978**, *17*, 3334.
(8) Tai, Z. H.; Zhang, G. C.; Qian, X. P.; Xiao, S. J.; Lu, Z. H.; Wei, Y. *Langmuir* **1993**, *9*, 1601.
(9) Liu, X. H.; Abser, N.; Bruce, D. W. *J. Organomet. Chem.* **1998**, *551*, 271.
(10) Buncel, E.; Keum, S. R. *Tetrahedron* **1983**, *39*, 1091.
(11) Mastsui, M.; Tanaka, N.; Andoh, N.; Funabiki, K. *Chem. Mater.* **1998**, *10*, 1921.
(12) Sprintschnik, G.; Sprintschnik, H. W.; Kirsch, P. P.; Whitten, D. G. *J. Am. Chem. Soc.* **1977**, *99*, 4947.

10.1021/ic001326b CCC: $20.00
Published on Web 05/26/2001

Scheme 1. Structures of the Ligands

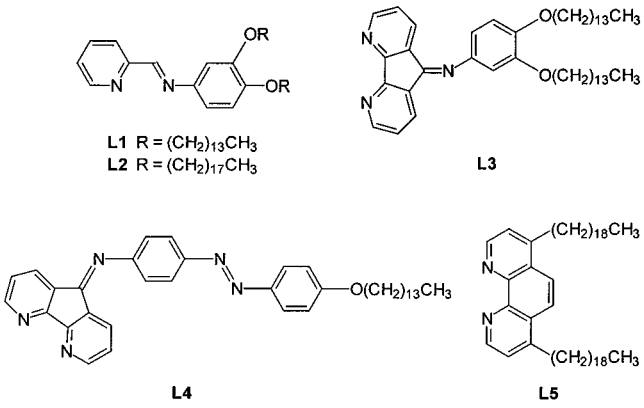

[Ru(bpy)$_2$L1](PF$_6$)$_2$ [L1 = *N*-(2-pyridylmethylene)-3,4-bis(tetradecyloxy)benzenamine] (1). To a refluxing ethanolic solution of 3,4-bis(tetradecyloxy)aniline (110 mg, 0.21 mmol) was added 2-pyridinecarboxaldehyde (23 mg, 0.21 mmol). The solution was heated and stirred for 5 min and then *cis*-[Ru(bpy)$_2$Cl$_2$] (100 mg, 0.19 mmol) was added. The mixture was refluxed overnight under nitrogen. After cooling to room temperature, the solution was filtered and reduced in volume. A saturated solution of NH_4PF_6 in methanol was added. The desired product was obtained by filtration and recrystallization by vapor diffusion of diethyl ether into an acetonitrile solution of the complex. Yield: 75%. Elemental analyses [$C_{60}H_{82}F_{12}N_6O_2P_2Ru$] calcd (found): C 55.00 (55.02), H 6.31 (6.21), N 6.41 (6.13). ^{1}H NMR (300 MHz, $CDCl_3$, 298 K): δ 0.9 (t, J = 6.5 Hz, 6H, CH_3), 1.3 (m, 44H, CH_2), 1.6 (q, J = 6.5 Hz, 4H, CH_2), 3.5 (m, 2H, OCH_2), 3.8 (m, 2H, OCH_2), 6.0 (d, J = 2.5 Hz, 1H, aromatic H), 6.1 (dd, J = 8.0 Hz, J = 2.5 Hz, 1H, aromatic H), 6.5 (d, J = 8.0 Hz, 1H, aromatic H), 7.2 (t, J = 5.0 Hz, 1H, pyridyl H), 7.4−7.6 (t, J = 5.0 Hz, 4H, pyridyl H), 7.6−7.7 (d, J = 5.0 Hz, 2H, pyridyl H), 7.7−7.8 (m, 3H, pyridyl H), 8.0 (m, 4H, pyridyl H), 8.1 (m, 1H, pyridyl H), 8.2−8.3 (d, J = 8.0 Hz, 2H, pyridyl H), 8.5 (m, 3H, pyridyl H), 9.0 (s, 1H, CH═N). Positive ESI-MS: m/z 1165 {M − PF_6}$^+$, 511 {M − 2PF_6}$^{2+}$.

[Ru(bpy)$_2$L2](PF$_6$)$_2$ [L2 = *N*-(2-pyridylmethylene)-3,4-bis(octadecyloxy)benzenamine] (2). The complex was prepared by the same procedure to that described for **1** with 3,4-bis(octadecyloxy)aniline used instead of 3,4-bis(tetradecyloxy)aniline. Yield: 80%. Elemental analyses [$C_{68}H_{98}F_{12}N_6O_2P_2Ru$] calcd (found): C 57.41 (57.45), H 6.94 (6.99), N 5.91 (5.82). ^{1}H NMR (300 MHz, $CDCl_3$, 298 K): δ 0.9 (t, J = 6.5 Hz, 6H, CH_3), 1.3 (m, 60H, CH_2), 1.7 (q, J = 6.5 Hz, 4H, CH_2), 3.6 (m, 2H, OCH_2), 3.9 (m, 2H, OCH_2), 6.0 (d, J = 2.5 Hz, 1H, aromatic H), 6.1 (dd, J = 8.0 Hz, J = 2.5 Hz, 1H, aromatic H), 6.5 (d, J = 7.0 Hz, 1H, aromatic H), 7.2−7.5 (t, J = 5.0 Hz, 4H, pyridyl H), 7.5−7.7 (m, 6H, pyridyl H), 8.0−8.1 (m, 5H, pyridyl H), 8.2−8.3 (d, J = 8.0 Hz, 2H, pyridyl H), 8.6 (m, 3H, pyridyl H), 9.0 (s, 1H, CH═N). Positive ESI-MS: m/z 1278 {M − PF_6}$^+$, 567 {M − 2PF_6}$^{2+}$.

[Ru(bpy)$_2$L3](PF$_6$)$_2$ (3). A mixture of *cis*-[Ru(bpy)$_2$Cl$_2$] (100 mg, 0.19 mmol) and **L3** (144 mg, 0.21 mmol) in absolute ethanol was heated to reflux for 8 h. After cooling to room temperature, the solution was filtered and the filtrate was reduced in volume. A saturated solution of NH_4PF_6 in methanol was added. The desired product was obtained by filtration and recrystallization by vapor diffusion of diethyl ether into an acetonitrile solution of the complex. Yield: 80%. Elemental analyses [$C_{65}H_{83}F_{12}N_7O_2P_2Ru\cdot0.5(H_2O)$] calcd (found): C 55.99 (55.74), H 6.07 (6.18), N 7.03 (7.30). ^{1}H NMR (300 MHz, $CDCl_3$, 298 K): δ 0.9 (t, J = 6.5 Hz, 6H, CH_3), 1.2−1.5 (m, 44H, CH_2), 1.8 (q, J = 6.5 Hz, 4H, CH_2), 3.9 (t, J = 6.0 Hz, 2H, CH_2), 4.0 (t, J = 6.0 Hz, 2H, CH_2), 6.7 (dd, J = 8.0 Hz, J = 2.5 Hz, 1H, aromatic H), 6.8 (d, J = 2.5 Hz, 1H, aromatic H), 7.0 (d, J = 8.0 Hz, 1H, aromatic H), 7.2 (m, 1H, pyridyl H), 7.4−7.6 (m, 7H, pyridyl H), 7.7 (d, J = 5.0 Hz, 1H, pyridyl H), 7.9 (t, J = 5.0 Hz, 2H, pyridyl H), 8.0−8.2 (m, 6H, pyridyl H), 8.3 (d, J = 7.5 Hz, 1H, pyridyl H), 8.7 (m, 4H, pyridyl H). Positive ESI-MS: m/z 1241 {M − PF_6}$^+$, 548 {M − 2PF_6}$^{2+}$.

[Ru(bpy)$_2$L4](PF$_6$)$_2$ (4). The complex was prepared with the same methodology as that described for **3**, except **L4** (120 mg, 0.21 mmol) was used instead of **L3**. Yield: 65%. Elemental analyses [$C_{57}H_{59}F_{12}N_9OP_2Ru$] calcd (found): C 53.61 (53.77), H 4.66 (4.39), N 9.87 (10.02). ^{1}H NMR (300 MHz, $CDCl_3$, 298 K): δ 0.9 (t, J = 6.5 Hz, 3H, CH_3), 1.3−1.5 (m, 22H, CH_2), 1.8 (t, J = 6.5 Hz, 2H, CH_2), 4.0 (t, J = 6.5 Hz, 2H, CH_2), 6.7 (d, J = 6.0 Hz, 2H, aromatic H), 7.0 (d, J = 2.0 Hz, 2H, aromatic H), 7.2 (t, J = 5.0 Hz, 2H, aromatic H), 7.4 (t, J = 5.0 Hz, 2H, pyridyl H), 7.5−8.2 (m, 18H, pyridyl H), 8.4 (d, J = 7.5 Hz, 1H, pyridyl H), 8.6 (m, 3H, pyridyl H). Positive ESI-MS: m/z 1132 {M − PF_6}$^+$, 494 {M − 2PF_6}$^{2+}$.

[Ru(bpy)$_2$L5](PF$_6$)$_2$ (5). The complex was prepared by the same procedure as that described for **3**, except **L5** (145 mg, 0.21 mmol) was used instead of **L3**. Yield: 85%. Elemental analyses [$C_{70}H_{100}F_{12}N_6P_2Ru$] calcd (found): C 59.34 (59.55), H 7.12 (6.97), N 5.93 (5.85). ^{1}H NMR (300 MHz, $CDCl_3$, 298 K): δ 0.9 (t, J = 6.5 Hz, 6H, CH_3), 1.2−1.8 (m, 78H, CH_2), 3.3 (t, J = 7.0 Hz, 4H, CH_2), 7.2 (t, J = 7.0 Hz, 2H, aromatic H), 7.4 (t, J = 6.0 Hz, 2H, aromatic H), 7.5 (dd, J = 6.0 Hz, J = 4.0 Hz, 4H, aromatic H), 7.8 (d, J = 5.0 Hz, 2H, aromatic H), 7.9 (d, J = 5.0 Hz, 2H aromatic H), 8.0 (t, J = 7.5 Hz, 2H, aromatic H), 8.1 (t, J = 7.5 Hz, 2H aromatic H), 8.4 (s, 2H, aromatic H), 8.5 (t, J = 7.0 Hz, 4H, aromatic H). Positive ESI-MS: m/z 1272 {M − PF_6}$^+$, 564 {M − 2PF_6}$^{2+}$.

[Ru(L5)$_3$](PF$_6$)$_2$ (6). A mixture of $RuCl_3\cdot3H_2O$ (50 mg, 0.19 mmol) and **L5** (446 mg, 0.63 mmol) with a few drops of triethylamine in ethanol was heated to reflux for 12 h. The mixture was cooled and filtered. A saturated solution of NH_4PF_6 in methanol was added. The desired product was obtained by filtration and recrystallization by vapor diffusion of diethyl ether into an acetonitrile solution of the complex. Yield: 60%. Elemental analyses [$C_{150}H_{252}F_{12}N_6P_2Ru$] calcd (found): C 71.19 (70.98), H 10.04 (10.01), N 3.32 (3.43). ^{1}H NMR (300 MHz, $CDCl_3$, 298 K): δ 0.9 (t, J = 6.5 Hz, 18H, CH_3), 1.2−1.5 (m, 192H, CH_2), 1.8 (m, 12H, CH_2), 3.3 (t, J = 5.5 Hz, 12H, CH_2), 7.6 (d, J = 5.5 Hz, 6H, phen H), 8.0 (d, J = 5.5 Hz, 6H, phen H), 8.3 (s, 6H, phen H). Positive ESI-MS: m/z 1121 {M − 2PF_6}$^{2+}$.

Physical Measurements and Instrumentation. Electronic absorption spectra were recorded on a Hewlett-Packard 8452A diode-array spectrophotometer. Steady state emission and excitation spectra at room temperature and 77 K were recorded on a Spex Fluorolog-2 Model F 111 fluorescence spectrophotometer. Solution samples were rigorously degassed with no fewer than four freeze−pump−thaw cycles prior to the measurements. Solid state photophysical studies were carried out with solid samples contained in a quartz tube inside a quartz-walled Dewar flask. Measurements of the EtOH−MeOH (4:1, v/v) glass or solid state samples at 77 K were similarly conducted with liquid nitrogen filled in the optical Dewar flask. Excited-state lifetimes of solid and solution samples were measured using a conventional laser system. The excitation source was the 355-nm output (third harmonic, 8 ns) of a Quanta-Ray Q-switched GCR-150 pulsed Nd:YAG laser (10 Hz). Luminescence decay traces were recorded on a Tektronix Model TDS 620A digital oscilloscope, and the lifetime (τ) determination was accomplished by single-exponential fitting of the luminescence decay traces with the model $I(t) = I_o \exp(-t/\tau)$, where $I(t)$ and I_o stand for the luminescence intensity at time = t and time = 0, respectively. ^{1}H NMR spectra were recorded on a Bruker DPX-300 (300 MHz) FT-NMR spectrometer. All ESI mass spectra were recorded on a Finnigan MAT95 mass spectrometer. Cyclic voltammetric measurements were performed by using a CH Instruments, Inc. Model CHI 620 Electrochemical Analyzer. Electrochemical measurements were performed in acetonitrile solutions with 0.1 mol dm^{-3} ^{n}Bu$_4$NPF$_6$ as supporting electrolyte at room temperature. The reference electrode was a Ag/$AgNO_3$ (0.1 M in acetonitrile) electrode and the working electrode was a glassy carbon (Atomergic Chemetal V25) electrode with a piece of platinum wire as counter electrode in a compartment that is separated from the working electrode by a sintered glass frit. The ferrocenium/ferrocene couple ($FeCp_2^{+/0}$) was used as the internal reference.[13a] Treatment of the electrode surfaces was the same as a reported procedure.[13b] All solutions for electrochemical studies were deaerated with prepurified argon gas before measurements. Elemental analyses

(13) (a) Gagne, R. R.; Koval, C. A.; Lisensky, G. C. *Inorg. Chem.* **1980**, *19*, 2854. (b) Che, C. M.; Wong, K. Y.; Anson, F. C. *J. Electroanal. Chem., Interfacial Electrochem.* **1987**, *226*, 211.

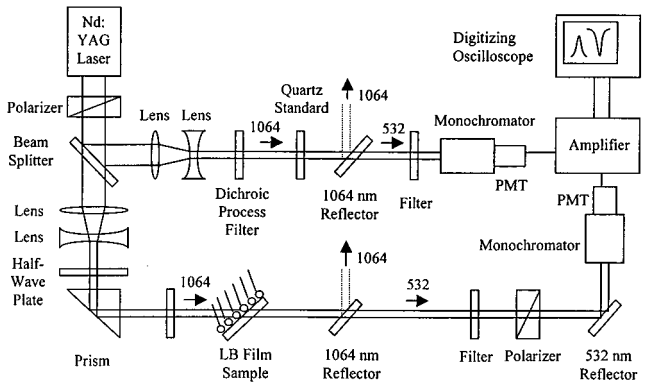

Figure 1. Schematic diagram of the experimental setup for SHG measurement.

of all the metal complexes were performed on a Carlo Erba 1106 elemental analyzer by the Institute of Chemistry at the Chinese Academy of Sciences in Beijing.

Pressure−area (π−A) isotherms and Langmuir−Blodgett (LB) Film Deposition. Pressure−area isotherms of all complexes were recorded on a Nima model-622 computer-controlled trough. Ultrapure water was obtained from an Elga UHQ PS apparatus. Water was obtained with resistivity greater than 18 MΩ cm and was used immediately. All complexes were dissolved in dichloromethane with a concentration of ca. 1 mg cm^{-3}. The solution was spread onto an ultrapure water subphase and was allowed to evaporate for at least 15 min. The surface pressure−area isotherms were recorded with a barrier compression speed of 150 cm^2 min^{-1}. For the monolayer preparation, the quartz substrate was made hydrophilic by consecutive sonication in detergent for 30 min and then soaking in both chromic acid and piranha solution (30% H_2O_2−H_2SO_4, 3:7, v/v) for 12 h. The treated substrate was washed thoroughly with ultrapure water just before use. The monolayer was transferred onto the treated quartz substrate at a constant pressure of 25 mN m^{-1} and dipping speed of 3 mm min^{-1}. All complex LB films are Z-type. The trough was cleaned after deposition of each layer and the deposition steps were repeated. All film layers had transfer ratios close to unity.

Second-Harmonic-Generation (SHG) Measurements. The setup for SHG measurements (Figure 1) was similar to that reported previously.[14] A fundamental laser light (1064 nm) from a Quanta-Ray Q-switched GCR-150−10 pulsed Nd:YAG laser was polarized either parallel (*p*) or perpendicular (*s*) to the plane of incidence using a Glan-Taylor polarizer and a half-wave plate. A Y-cut quartz crystal was used as the reference. The polarized light beam was focused by a quartz convex lens (50 mm focal length). A dichroic process filter was inserted before the sample holder to eliminate possible SHG (532 nm) generated from optical components. The laser beam was directed at an incident angle of 45° onto the monolayer film mounted vertically on a sample holder. The SHG signal generated by the sample was detected by a photomultiplier tube (PMT, Hamamatsu-1P28) with a high-voltage power supply (Oriel-70705). The output signal was amplified by a preamplifier (EG&G Instruments, 5185 wideband preamplifier) and recorded on a Tektronix TDS-620A digital oscilloscope. The laser power was monitored by a PMT in the reference path to ensure that the same incident laser power was used for all measurements.

Results and Discussion

Electronic Absorption Spectroscopy. The electronic absorption data are listed in Table 1. All complexes show intense absorption peaks at ca. 200−300 nm and are assigned to intraligand (IL) transition. The shoulders at ca. 300−400 nm originated from the low-energy components of the IL bands.

Table 1. Photophysical Data for Complexes **1**−**6**

complex	medium (T/K)	emission λ_{em}/nm[a,b] (τ_o/μs)	absorption λ_{abs}/nm[c] (ϵ/dm^3 mol^{-1} cm^{-1})
1	CH_3CN (298)	782 (<0.1)	244 (26060), 288 (51170),
	solid (298)	734	345 sh (8710), 382 sh (8900),
	solid (77)	726	426 (10240), 480 sh (9050)
	glass[d] (77)	712	
2	CH_3CN (298)	780 (<0.1)	242 (25850), 286 (48830),
	solid (298)	733	346 sh (9070), 382 sh (8800),
	solid (77)	725	426 (11300), 480 sh (9360)
	glass[d] (77)	717	
3	CH_3CN (298)	627 (1.05)[e]	238 (62610), 286 (72190),
	solid (298)	610[e]	322 sh (18580), 422 sh
	solid (77)	591[e]	(18510), 448 (19150)
	glass[d] (77)	573[e]	
4	CH_3CN (298)	620 (0.99)[e]	242 (47040), 286 (75010),
	solid (298)	586[e]	322 sh (21390), 420 sh
	solid (77)	588[e]	(16480), 440 (19040)
	glass[d] (77)	569[e]	
5	CH_3CN (298)	625 (1.05)	266 (75520), 288 (70190),
	solid (298)	610	384 sh (9350), 426 (16410),
	solid (77)	600	452 (18170)
	glass[d] (77)	598	
3	CH_3CN (298)	604 (1.42)	266 (99680), 450 (17160)
	solid (298)	609	
	solid (77)	594	
	glass[d] (77)	582	

[a] Emission maxima are corrected values. [b] Excitation wavelength at 500 nm. [c] In acetonitrile at 298 K. [d] EtOH−MeOH (4:1, v/v). [e] Excitation wavelength at 400 nm.

With reference to previous spectroscopic studies of ruthenium(II) complexes with diimine ligands,[15,16] the bands with maximum absorptions at ca. 426 nm of **1** and **2** are assigned to an admixture of the $\pi\rightarrow\pi^*$ IL and dπ(Ru)$\rightarrow\pi^*$(bpy) MLCT transitions, while the shoulders at ca. 480 nm are assigned to the dπ(Ru)$\rightarrow\pi^*$(diimine) MLCT transition. An admixture of the $\pi\rightarrow\pi^*$ IL transition and dπ(Ru)$\rightarrow\pi^*$(bpy) MLCT, and dπ(Ru)$\rightarrow\pi^*$(diimine) MLCT transitions are observed at 422 and 448 nm for **3**. Similar absorption bands are noticed at 420 and 440 nm for **4**. The MLCT energies of these two complexes are similar to those found in related complexes.[17] Compound **5** displays strong absorption bands at ca. 426 and 452 nm, which are tentatively assigned as an admixture of the $\pi\rightarrow\pi^*$ IL, dπ(Ru)$\rightarrow\pi^*$(bpy) MLCT, and dπ(Ru)$\rightarrow\pi^*$(**L5**) MLCT transitions. Similarly, the homoleptic complex **6** shows an admixture of the $\pi\rightarrow\pi^*$ IL and dπ(Ru)$\rightarrow\pi^*$(**L5**) MLCT transitions at 450 nm and is similar to those found in other ruthenium(II) complexes with alkyl-substituted phenanthroline ligands.[18]

Emission Spectroscopy. The emission data are shown in Table 1. Excitation of all the complexes at λ > 350 nm produced a red emission, which is assigned as originating from the lowest energy triplet MLCT state. The emission energy of **1** and **2** in acetonitrile (ca. 780 nm) was similar to those of related complexes.[15] The much lower emission energies of these complexes than that of $[Ru(bpy)_3]^{2+}$ (613 nm)[19] are suggestive of an emissive origin of the dπ(Ru)$\rightarrow\pi^*$(diimine) MLCT triplet

(14) (a) Dougherty, J. P.; Kurt, S. K. *J. Appl. Crystallogr.* **1976**, *9*, 145. (b) Girling, I. R.; Cade, N. A.; Kolinsky, P. V.; Peterson, I. R.; Ahmad, M. M.; Neal, D. B.; Petty, M. C.; Roberts, G. G.; Feast, W. J. *J. Opt. Soc. Am. B* **1987**, *4*, 950. (c) Yam, V. W. W.; Wang, K. Z.; Wang, C. R.; Yang, Y.; Cheung, K. K. *Organometallics* **1998**, *17*, 2440.

(15) Brown, G. M.; Weaver, T. R.; Keene, F. R.; Meyer, T. J. *Inorg. Chem.* **1976**, *15*, 190.

(16) Yam, V. W. W.; Lee, V. W. M. *J. Chem. Soc., Dalton Trans.* **1997**, 3005.

(17) Wang, Y.; Perez, W.; Zheng, G. Y.; Rillema, D. P. *Inorg. Chem.* **1998**, *37*, 2051.

(18) Blakley, R. L.; Myrick, M. L.; Pittman, R.; De Armond, M. K. *J. Phys. Chem.* **1990**, *94*, 4804.

(19) (a) Crosby, G. A.; Perkins, W. G.; Klassen, D. M. *J. Chem. Phys.* **1965**, *43*, 1498. (b) Kalyanasundaram, K. *Coord. Chem. Rev.* **1982**, *46*, 159, and references therein. (c) Juris, A. J.; Balzani, V.; Belser, P.; von Zelewsky, A. *Helv. Chim. Acta* **1981**, *64*, 2175.

Table 2. Electrochemical Data for Complexes **1**−**6**[a]

	$E_{1/2}$[b]/V vs SCE			$E_{1/2}$[b]/V vs SCE	
complex	oxidation	reduction	complex	oxidation	reduction
1	+1.31	−1.07	**4**	+1.38	−0.64
		−1.57			−1.54
		−1.76			−1.74
2	+1.32	−1.06	**5**	+1.22	−1.38
		−1.57			−1.50
		−1.79	**6**	+1.19	−1.32
3	+1.38	−0.67			−1.42
		−1.55			
		−1.72			

[a] In acetonitrile solution with 0.1 mol dm^{-3} ^{n}Bu$_4$NPF$_6$ (TBAH) as supporting electrolyte at room temperature; scan rate 100 mV s^{-1}. [b] $E_{1/2}$ refers to $(E_{pa} + E_{pc})/2$, where E_{pa} and E_{pc} are the anodic and cathodic peak potentials, respectively.

states as the π^* orbitals of the diimine ligands are lower lying in energy than that of 2,2′-bipyridine. Complexes **3** and **4** emit at ca. 627 and 620 nm in acetonitrile, respectively, similar to that reported for $[Ru(bpy)_2(dafo)]^{2+}$ (dafo = 4,5-diazafluoren-9-one),[17] which emits at ca. 630 nm. Complex **5** luminesces strongly at 625 nm and is red-shifted by ca. 0.08 eV from that of $[Ru(bpy)_2(phen)]^{2+}$ (600 nm).[20] Such a red shift in emission energy could be attributed to the stronger σ-donating ability and the weaker π-accepting ability of **L5** than phen, which destabilizes the dπ orbital of ruthenium and gives rise to a lower energy ^{3}MLCT [dπ(Ru)→π^*(bpy)] emission. Similarly, the ^{3}MLCT emission of complex **6** occurs at a lower energy (604 nm) than that of the corresponding $[Ru(phen)_3]^{2+}$ complex (588 nm).[20] In general, the bathochromic shifts of **5** and **6** with respect to the phen analogues have been ascribed to the better σ-donating ability as well as the slightly poorer π-accepting ability of **L5** than phen, rendering the dπ orbital of the ruthenium(II) metal center higher lying in energy.

Electrochemical Properties. The electrochemical data for all complexes are listed in Table 2. For **1**−**4**, quasi-reversible Ru(II)/(III) oxidation couples are found at +1.31 to +1.38 V vs SCE. Reversible reduction couples between −1.5 and −1.8 V vs SCE are assigned to the successive one-electron reductions of the bipyridine ligands. With reference to previous studies on similar systems,[15] quasi-reversible reduction couples at ca. −1.07 V vs SCE of **1** and **2** are assigned to reductions of the respective diimine ligands **L1** and **L2**. The almost identical electrochemical behavior of **1** and **2** can be ascribed to virtually the same structures of both complexes and little difference in inductive effects between tetradecyl and octadecyl hydrocarbon chains. For **3** and **4**, the reduction potentials at −0.67 and −0.64 V vs SCE, respectively, are assigned to the one-electron reduction of the diazafluorene ligands, similar to that found in $[Ru(bpy)_2(dafo)](PF_6)_2$ (−0.65 V vs SCE).[17] In the cyclic voltammogram of **5**, reversible reduction couples are found to occur at −1.38 and −1.50 V vs SCE and are assigned to the ligand-centered reductions of bpy and **L5**, respectively. Quasi-reversible oxidation of Ru(II) to Ru(III) is observed at +1.22 V vs SCE, which is slightly less positive than that of $[Ru(bpy)_3]^{2+}$ (+1.28 V vs SCE).[21] Replacement of a bipyridyl ligand in $[Ru(bpy)_3]^{2+}$ by the better σ-donating and poorer π-accepting ligand **L5** would raise the dπ(Ru) orbital energy, leading to the increased ease of metal-centered oxidation. Two reversible reduction waves are located at −1.32 and −1.42 V vs SCE for **6**. They are assigned as the two closely spaced one-electron reductions of the ligand **L5**. A quasi-reversible Ru(II)/(III) oxidation couple at +1.19 V vs SCE is observed. The less positive $E°(Ru^{III/II})$ value relative to that of $[Ru(bpy)_3]^{2+}$ by ca. 100 mV is again indicative of the greater ease of oxidation of the ruthenium(II) metal center, resulted from the slightly poorer π-accepting ability and better σ-donating ability of **L5** than bpy.

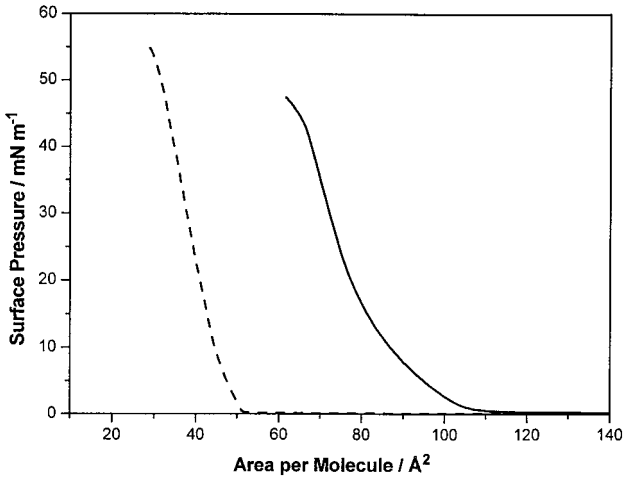

Figure 2. Surface pressure−area (π−A) isotherms of **3** (−) and **4** (---).

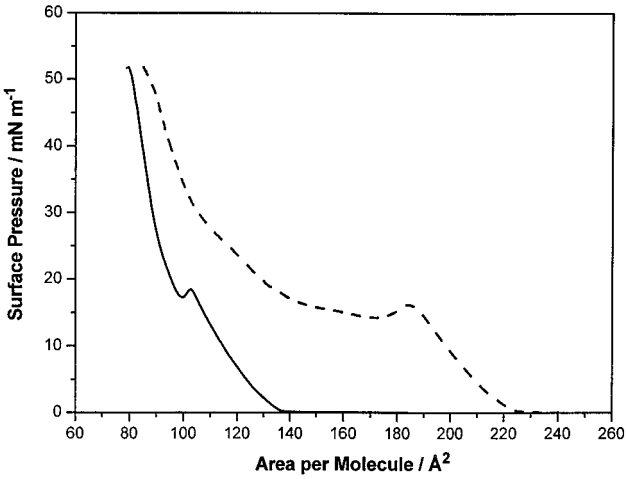

Figure 3. Surface pressure−area (π−A) isotherms of **5** (−) and **6** (---).

Table 3. Langmuir−Blodgett (LB) Film-Forming Properties for Complexes **1**−**6**

complex	molecular area/Å^2	collapse pressure/mN m^{-1}
1	85	>58
2	105	>58
3	87	>43
4	47	>53
5	130	>50
6	219	>52

Surface Pressure−Area (π−A) Isotherm. The π−A isotherms of all the complexes spread from dichloromethane solutions onto ultrapure water at room temperature were recorded, and the data are summarized in Table 3. The surface pressure−area isotherms of **3**−**6** are shown in Figures 2 and 3. The fairly similar collapse pressures and hence film stabilities of **1** and **2** are expected as a result of the similarity in their structures. Compound **3** displays a π−A isotherm with more well-defined phase transitions and its surface area per molecule nearly doubles that of **4**, which can be accounted for by the

(20) Caspar, J. V.; Meyer, T. J. *Inorg. Chem.* **1983**, *22*, 2444.
(21) Tokel-Takvoryan, N. E.; Hemingway, R. E.; Bard, A. J. *J. Am. Chem. Soc.* **1973**, *95*, 6582.

Table 4. Multilayer LB Film-Forming Properties for Complexes **1**−**5**

complex	absorbance/ layer	surface concentration: calcd by Lambert−Beer law/mol cm^{-2}	surface concentration: calcd from A_o/mol cm^{-2}
1	2.61×10^{-3}	2.8×10^{-10}	1.9×10^{-10}
2	2.17×10^{-3}	2.4×10^{-10}	1.5×10^{-10}
3	6.74×10^{-3}	3.5×10^{-10}	1.9×10^{-10}
4	6.23×10^{-3}	3.2×10^{-10}	3.5×10^{-10}
5	1.73×10^{-3}	0.9×10^{-10}	1.2×10^{-10}

steric requirements of the two hydrocarbon tails in the former instead of one in the latter. The $\pi-A$ isotherm of **4** exhibits a steep rise in surface pressure with a high collapse pressure of ca. 53 mN m^{-1}. This observation, together with the small molecular area, when compared to ca. 80−90 Å^2 per molecule found in other ruthenium(II) bipyridyl surfactants,[22] indicates the formation of a condensed, stable monolayer in the air−water interface. For **5** and **6**, two noticeable phase transitions are observed. The first transition that occurs at low surface pressure is due to the formation of the monolayer from the gaseous phase, whereas the second one at higher surface pressure is a result of the aggregation of monolayers and multilayer structure formation. The larger surface area of **5**, when compared to that of **2**, can be rationalized by the fact that the two hydrocarbon chains on **5** are on the 4- and 7-positions of the phenanthroline ligand, which are more spacially separated than those attached to the same phenyl ring in **2**. The large surface area (219 Å^2 per molecule) of **6** suggests that the molecules may be lying parallel to the water−air interface, with the alkyl chains pointing upward serving as the hydrophobic portion and the central ruthenium(II) phenanthroline moiety as the hydrophilic portion of the amphiphilic species in the resulting film.[3,23]

Langmuir−Blodgett (LB) Film Deposition. The surface concentration of the complexes on the LB film can be derived from the Lambert−Beer law modified for two-dimensional concentration[24]

$$\Gamma = D/1000\epsilon \tag{1}$$

where Γ is the surface concentration (mol cm^{-2}), D is the absorbance per layer (AU/layer), and ϵ is the molar extinction coefficient (dm^3 mol^{-1} cm^{-1}) at a particular wavelength. D can be obtained from the slope of a linear plot of absorbance against the number of layers for a given complex. The surface concentration can also be calculated from the limiting surface area (A_o) determined by the extrapolation of the linear part to zero surface pressure in the $\pi-A$ isotherm by the equation[24]

$$\Gamma = 10^{16}/A_oN \tag{2}$$

in which Γ is the surface concentration (mol cm^{-2}), A_o is the limiting surface area (Å^2), and N is Avogadro's number. The multilayer LB film forming properties of the complexes are summarized in Table 4. The electronic absorption spectral traces of **4** deposited on a quartz substrate are shown in Figure 4.

Complexes **1**−**5** show a linear relationship between the absorbance and the layer number. The surface concentrations calculated by both methods are consistent with each other. This shows that the complex monolayers are regularly transferred onto the quartz substrates. In general, the smaller the molecule is, the higher the surface concentration will be. It has been found that **6** exhibits a low transfer ratio, and no stable monolayer films of **6** were obtained on both hydrophilically and hydrophobically treated quartz substrates. These observations are consistent with the homoleptic octupolar characteristics of **6**.

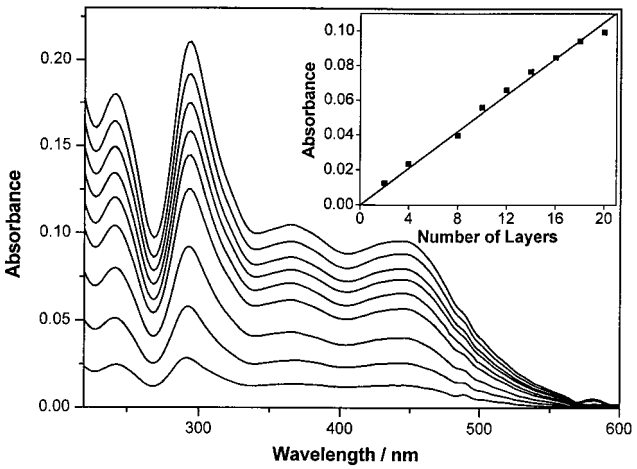

Figure 4. Electronic absorption spectral traces of 2 (bottom), 4, 8, 10, 12, 14, 16, 18, and 20 (top) layers of complex **4** deposited on a quartz substrate. The insert shows a plot of absorbance at 448 nm vs number of deposited layers.

Nonlinear Optical Properties. The calculation for the first-order molecular hyperpolarizability (β) was based on the general procedure described by Ashwell and co-workers.[25] By assuming that all the molecules on the quartz substrate have a common tilt angle ϕ to the normal of the plane with a random azimuthal distribution and that β is dominated by the resultant donor−acceptor components, the following equations can be obtained:

$$\frac{I_{2\omega,p\rightarrow p}}{I_{2\omega,s\rightarrow p}} = \frac{(\chi^{(2)}_{zzz}\sin^3\theta + 3\chi^{(2)}_{zxx}\sin\theta\cos^2\theta)^2}{(\chi^{(2)}_{zxx}\sin\theta)^2} \tag{3}$$

$$\chi^{(2)}_{zzz} = \chi^{(2)}\cos^3\phi = Nf_{2\omega}(f_\omega)^2\beta\cos^3\phi \tag{4}$$

$$\chi^{(2)}_{zxx} = 0.5\chi^{(2)}\cos\phi\sin^2\phi = 0.5Nf_{2\omega}(f_\omega)^2\beta\cos\phi\sin^2\phi \tag{5}$$

where $\theta = 45°$ is the angle of the laser beam to the film, ϕ is the tilt angle of the chromophore to the normal of the substrate, $I_{2\omega,p\rightarrow p}$ is the p-polarized double-frequency signal intensity with p-polarized incident fundamental light, $I_{2\omega,s\rightarrow p}$ is the p-polarized double-frequency signal intensity with s-polarized incident fundamental light, s and p stand for vertical and parallel to the plane of incidence, $f_{\omega,2\omega} = [(n_{\omega,2\omega})^2 + 2]/3$ is a local field correction factor, where n_ω and $n_{2\omega}$ are the refractive indices of the film at the fundamental and second-harmonic frequencies, respectively. $n_{2\omega}$ is usually higher than n_ω. In actual treatment, n_ω and $n_{2\omega}$ are taken to be 1.5 or 1.7, $\chi^{(2)}_{zzz}$ and $\chi^{(2)}_{zxx}$ are the two independent components characterized by the substrate normal (z) and the plane of film surface (xy), and $N = 1/(Al)$ is the number of molecules per unit volume, where l is the film thickness and A the molecular area of the film-forming materials under study. Substituting eqs 4 and 5 into 3 gave eq 6, from

(22) Johansen, O.; Kowala, C.; Mau, A. W. H.; Sasse, W. H. F. *Aust. J. Chem.* **1979**, *32*, 1453.
(23) Kalina, D. W.; Crane, S. W. *Thin Solid Films* **1985**, *109*, 134.
(24) Taniguchi, T.; Fukasawa, Y.; Miyashita, T. *J. Phys. Chem. B* **1999**, *103*, 1920.
(25) Ashwell, G. J.; Hargreaves, R. C.; Baldwin, C. E.; Bahra, G. S.; Brown, C. R. *Nature* **1992**, *357*, 393.

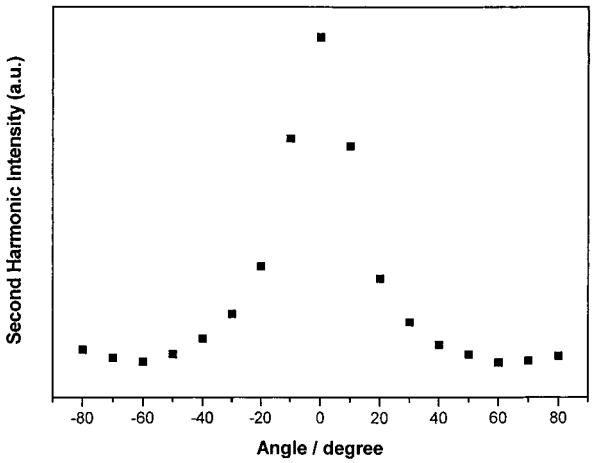

Figure 5. Normalized SHG intensity vs. polarization angle from a monolayer film of complex **3**.

which the tilt angle ϕ can be calculated:

$$\tan \phi = [(I_{2\omega,p\rightarrow p}/I_{2\omega,s\rightarrow p})^{1/2} - 3/2]^{-1/2} \quad (6)$$

By using the tilt angle ϕ calculated by eq 6 and comparing the $I_{2\omega,p\rightarrow p}$ and $I_{2\omega,s\rightarrow p}$ signals with the envelope maximum ($d_{11} = 1.2 \times 10^{-9}$ esu) of a Y-cut quartz crystal reference at 0° incidence angle, the values of $\chi^{(2)}$ and β can be obtained by using the following equations:

$$\chi^{(2)}_{s,zxx} = (I_{2\omega,s\rightarrow p}/I_{Q,2\omega})^{1/2} \times 2.8 \times 10^{-11} \quad (7)$$

$$\chi^{(2)}_{zxx} = \chi^{(2)}_{s,zxx}/l = 0.5\chi^{(2)} \cos \phi \sin^2 \phi \quad (8)$$

$$\chi^{(2)} = Nf_{2\omega}(f_\omega)^2\beta \quad (9)$$

in which $\chi^{(2)}_{s,zxx}$ is the second-order susceptibility $\chi^{(2)}$ on the plane of the film.

By substituting eq 8 into 9 and making β as the subject, eq 10 resulted.

$$\beta = \frac{\chi^{(2)}_{s,zxx}A}{0.5\chi^{(2)}f_{2\omega}(f_\omega)^2 \cos \phi \sin^2 \phi} \quad (10)$$

Complexes **3** and **4** were found to show SHG properties. Figure 5 shows a plot of SHG signals as a function of the polarization angle of **3**. The peaks and troughs correspond to the double-frequency signal from *p*-polarized ($I_{2\omega,p\rightarrow p}$) and *s*-polarized ($I_{2\omega,s\rightarrow p}$) fundamental beams, respectively, while the *x*-axis corresponds to the angle of rotation of the half-wave plate. The molecular tilt angles and first molecular hyperpolarizabilities are tabulated in Table 5. (*E*)-*N*-Methyl-4-(2-(4-octadecyloxyphenyl)ethenyl)pyridinium iodide (BI) is used as a standard ($\beta = 1.5 \times 10^{-28}$ esu)[26] for comparison. The transfer ratios of all monolayer films are close to unity. Both **3** and **4** have nearly the same tilt angles on the quartz substrates, which could be rationalized by the structural similarity of the diazafluorene ligands. The tilt angles are close to the 38° found by Yamada and co-workers[27] for various ruthenium(II) bipyridyl surfactants bearing tetradecyl and octadecyl alkyl chains. The molecular orientation and tilt angles are attributed to weak surface interactions of the hydrophobic headgroups with the solid substrates. The SHG intensities of **3** and **4** are ca. 3.6 and 2.6 times that of the standard BI, respectively. The large first molecular hyperpolarizabilities of **3** and **4** are likely due to the resultant component of the intramolecular charge transfer within the long chain diazafluorene ligand and the MLCT transitions, which has been demonstrated by Sakaguchi and co-workers[4a,b] with the SHG capabilities of other metal complexes with MLCT transitions. The presence of two electron-donating alkyloxy chains in **3** compared to one in **4** might produce a more pronounced donor−acceptor effect and account for the greater SHG activities of the former complex. When comparing **3** and **4** with **1, 2**, and **5**, it is found that only the ruthenium complexes with diazaflurorene ligands exhibit SHG behavior. This may be related to the structural configuration of the complex and the charge-transfer property of the long chain diimine ligand.

Table 5. Tilt Angles and First Molecular Hyperpolarizabilities of **3** and **4**

complex	molecular tilt angle, ϕ/deg	first molecular hyperpolarizability, β/esu	relative SHG intensity, β/β(BI)[a]
3	40	3.6×10^{-28}	3.6
4	39	2.7×10^{-28}	2.6

[a] BI [(*E*)-*N*-methyl-4-(2-(4-octadecyloxyphenyl)ethenyl)pyridinium iodide] is used as a standard for comparison.

Conclusion

Several amphiphilic ruthenium(II) surfactant complexes were synthesized and characterized. In general, they showed high collapse pressures which were very dependent on the structures and the chain lengths of the hydrocarbon tails. Complexes **1**−**5** exhibited good monolayer and multilayer film-forming properties. Complexes **3** and **4** were found to show SHG activities that are about 3.6 and 2.6 times of that of the organic standard BI.

Acknowledgment. V.W.-W.Y. acknowledges financial support from the Research Grants Council and The University of Hong Kong, and B.W.-K.C. the receipt of a Research Associateship from the Setting-Up Grant supported by the Vice-Chancellor's Development Fund of The University of Hong Kong.

IC001326B

(26) Lupo, D.; Prass, W.; Scheunemann, U.; Laschewsky, A.; Ringsdorf, H.; Ledoux, I. *J. Opt. Soc. Am. B.* **1988**, *5*, 300.
(27) Yamada, S.; Nakano, T.; Matsuo, T. *Thin Solid Films* **1994**, *245*, 196.